Calculation of nonzero-temperature Casimir forces in the time domain

Kai Pan, Alexander P. McCauley, Alejandro W. Rodriguez, M. T. Homer Reid, Jacob K. White, and Steven G. Johnson

Phys. Rev. A **83**, 040503 — Published 29 April 2011

DOI: 10.1103/PhysRevA.83.040503

Calculation of nonzero-temperature Casimir forces in the time domain

Kai Pan,[1,2] Alexander P. McCauley,[1] Alejandro W. Rodriguez,[1]
M. T. Homer Reid,[1,2] Jacob K. White,[2,3] and Steven G. Johnson[2,4]

[1] *Department of Physics, Massachusetts Institute of Technology, Cambridge, MA 02139, USA*
[2] *Research Laboratory of Electronics, Massachusetts Institute of Technology, Cambridge, MA 02139, USA*
[3] *Department of Electrical Engineering and Computer Science, Massachusetts Institute of Technology, Cambridge, MA 02139, USA*
[4] *Department of Mathematics, Massachusetts Institute of Technology, Cambridge, MA 02139, USA*

We show how to compute Casimir forces at nonzero temperatures with time-domain electromagnetic simulations, for example using a finite-difference time-domain (FDTD) method. Compared to our previous zero-temperature time-domain method, only a small modification is required, but we explain that some care is required to properly capture the zero-frequency contribution. We validate the method against analytical and numerical frequency-domain calculations, and show a surprising high-temperature disappearance of a non-monotonic behavior previously demonstrated in a piston-like geometry.

In this paper, we show how to compute nonzero-temperature ($T > 0$) corrections to Casimir forces via time-domain calculations, generalizing a computational approach based on the finite-difference time-domain (FDTD) method that we previously demonstrated for $T = 0$ [1, 2]. New computational methods for Casimir interactions [3–8] have become important in order to model non-planar micromechanical systems where unusual Casimir effects have been predicted, and there has been increasing interest in $T > 0$ corrections [9–19], especially in recently identified systems where these effects are non-negligible [12]. Although $T > 0$ effects are easy to incorporate in the imaginary frequency domain, where they merely turn an integral into a sum over Matsubara frequencies [20], they are nontrivial in time domain because of the singularity of the zero-frequency contribution, and we show that a naive approach leads to incorrect results. We validate using both a one-dimensional system where analytical solutions are available and also a two-dimensional (2D) piston-like geometry [3, 21] where we compare to a frequency-domain numerical method. In the piston, we observe an interesting effect in which a non-monotonic phenomenon previously identified at $T = 0$ disappears for a sufficiently large T.

The Casimir force arises from fluctuations at all frequencies ω, and the $T = 0$ force can be expressed as an integral $F(0) = \int_0^\infty f(\xi)d\xi$ over Wick-rotated imaginary frequencies $\omega = i\xi$ [20]. At $T > 0$, this integral becomes a sum over "Matsubara frequencies" $\xi_n = n\pi\omega_T$ for integers n, where $\omega_T = 2k_B T/\hbar$ and k_B is Boltzmann's constant [20]:

$$F(T) = \pi\omega_T \left[\frac{f(0^+)}{2} + \sum_{n=1}^{\infty} f\left(n\pi\omega_T\right) \right]. \tag{1}$$

Eq. (1) corresponds to a trapezoidal-rule approximation of the $T = 0$ integral [8]. At room temperature, $\xi = \pi\omega_T$ corresponds to a "wavelength" $2\pi/\xi = 7\,\mu$m, much larger than most experimental separations, so usually $T > 0$ corrections are negligible [20]. However, experiments are pushing towards $> 1\mu$m separations in attempts to measure this phenomenon [17, 18], recently culminating in an experiment at several μm that appears to clearly observe the $T > 0$ corrections [19]. Also, we have recently predicted much larger T corrections with certain materials and geometries [12].

Many of the recent techniques to compute Casimir forces in arbitrary geometries can be related to mature computational methods from classical electromagnetism (EM) [8]. One method is to use the fluctuation-dissipation theorem, by which the mean-square electric and magnetic fields $\langle E^2\rangle$ and $\langle H^2\rangle$ can be computed from classical Green's functions [20], and the mean stress tensor can be computed and integrated to obtain the force [1–3]. In particular, at each ω, the correlation function $\langle E^2\rangle$ is:

$$\langle E_j(\mathbf{x})E_k(\mathbf{x}')\rangle_\omega = -\frac{\hbar}{\pi}\,\mathrm{Im}\left[\omega^2 G^E_{jk}(\omega;\mathbf{x},\mathbf{x}')\right]\coth\left(\frac{\omega}{\omega_T}\right), \tag{2}$$

where $G^E_{jk} = (\mathbf{G}^E_k)_j$ is the classical dyadic "photon" Green's function, proportional to the electric field in the j direction at $\mathbf{x}$ due to an electric-dipole current in the k direction at $\mathbf{x}'$, and solves

$$\left[\nabla\times\mu(\omega,\mathbf{x})^{-1}\nabla\times - \omega^2\varepsilon(\omega,\mathbf{x})\right]\mathbf{G}^E_k(\omega,\mathbf{x},\mathbf{x}') = \delta^3(\mathbf{x}-\mathbf{x}')\hat{e}_k, \tag{3}$$

where ε is the electric permittivity tensor, μ is the magnetic permeability tensor, and $\hat{e}_k$ is a unit vector in direction k. The magnetic-field correlation $\langle H^2 \rangle$ has a similar form [1, 2]. Note that the temperature dependence appears as a coth factor (from a Bose-Einstein distribution). If this is Wick-rotated to imaginary frequency $\omega = i\xi$, the poles in the coth function gives the sum (1) over Matsubara frequencies [22]. In our EM simulation, what is actually computed is the electric or magnetic field in response to an electric or magnetic dipole current, respectively. This is related to G_{ij} by

$$E_{jk}(\omega, \mathbf{x}, \mathbf{x}') = -i\omega G^E_{jk}(\omega, \mathbf{x}, \mathbf{x}') \tag{4}$$

where $E_{jk}(\omega, \mathbf{x}, \mathbf{x}')$ denotes the electric field response in the jth direction due to a dipole current source $\mathbf{J}(\omega, \mathbf{x}, \mathbf{x}') = \delta(\mathbf{x} - \mathbf{x}')\hat{\mathrm{e}}_k$ [1].

This equation can be solved for each point on a surface to integrate the stress tensor, and for each frequency to integrate the contributions of fluctuations at all frequencies. Instead of computing each ω separately, one can use a pulse source in time, whose Fourier transform contains all frequencies. As derived elsewhere [1, 2], this corresponds to a sequence of time-domain simulations, where pulses of current are injected and some function $\Gamma(t)$ of the resulting fields (corresponding to the stress tensor) is integrated in time, multiplied by an appropriate weighting factor $g(t)$. We perform these simulations using the standard FDTD technique [23], which discretizes space and time on a uniform grid. In frequency domain, Wick rotation to complex $\omega(\xi)$ is crucial to obtain a tractable frequency integrand [3, 8], and the analogue in time domain is important to obtain rapidly decaying fields (hence short simulations) [1, 2]. In time domain, one must implement complex ω indirectly: because ω only appears explicitly with ε in Eq. (3), converting ω to the complex contour $\omega(\xi) \equiv \xi\sqrt{1 + \frac{i\sigma}{\xi}}$ is equivalent to operating at a real frequency ξ with an artificial conductivity $\varepsilon(\mathbf{r}) \to \varepsilon(\mathbf{r})(1 + \frac{i\sigma}{\xi})$ [1, 2]. (One cannot use purely imaginary frequencies $\omega = i\xi$ in time domain, because the corresponding material $\varepsilon \to -\varepsilon$ has exponentially growing solutions in time [1].) Thus, by adding an artificial conductivity everywhere, and including a corresponding Jacobian factor in $g(t)$, one obtains the same (physical) force result in a much shorter time (with the fields decaying exponentially due to the conductivity). (Note that the resulting "time" is not physical time but is instead a mathematical construction equivalent to a frequency-domain calculation for equilibrium or quasi-static problems.)

Now, we introduce the basic idea of how $T > 0$ is incorporated in the time domain, and explain where the difficulty arises. The standard $T > 0$ analysis of Eq. (1) is expressed in frequency domain, so we start there by exploiting the fact that the time-domain approach is derived from a Fourier transform of a frequency-domain approach. In particular, $g(t)$ is the Fourier transform of a weighting factor $g[\omega(\xi)]$ [1, 2]. At real ω, the effect of $T > 0$ is to include an additional factor $\coth\left[\frac{\omega(\xi)}{\omega_T}\right]$ in the $\omega(\xi)$ integral from Eq. (2). So, a naive approach is to replace $g[\omega(\xi)]$ with:

$$g[\omega(\xi)] \to g[\omega(\xi)] \coth\left[\frac{\omega(\xi)}{\omega_T}\right] = -i\xi\left(\sqrt{1 + \frac{i\sigma}{\xi}}\right)(1 + i\sigma/2\xi)\coth\left[\frac{\omega(\xi)}{\omega_T}\right], \tag{5}$$

using the $T = 0$ $g\left[\omega(\xi)\right]$ expression from Ref. 1, and then Fourier transform this to yield $g(t)$. However, there is an obvious problem with this approach: the $1/\omega$ singularity in $\coth\left[\frac{\omega(\xi)}{\omega_T}\right]$ means that Eq. (5) is not locally integrable around $\xi = 0$, and therefore its Fourier transform is not well-defined. If we naively ignore this problem, and compute the Fourier transform via a discrete Fourier transform, simply assigning an arbitrary finite value for the $\xi = 0$ term, this unsurprisingly gives an incorrect force for $T > 0$ compared to the analytical Lifshitz formula for the case of parallel perfect-metal plates in 1D [24], as shown in Fig. 1 (green dashed line).

Instead, a natural solution is to handle $\omega \neq 0$ by the coth factor as in Eq. (5), but to subtract the $\omega = 0$ pole and handle this contribution separately. We will extract the correct $\omega = 0$ contribution from the frequency-domain expression Eq. (1), convert it to time domain, and add it back in as a manual correction to $g(t)$. In particular, the $\coth\left[\frac{\omega(\xi)}{\omega_T}\right]$ function has poles at $\omega = in\pi\omega_T$ for integers n. When the ω integral is Wick-rotated, the residues of these poles give the Matsubara sum Eq. (1) via contour integration [22]. If we subtract the $n = 0$ pole from the coth, obtaining

$$g_{n>0}(\xi) = g[\omega(\xi)]\left\{\coth\left[\frac{\omega(\xi)}{\omega_T}\right] - \frac{\omega_T}{\omega(\xi)}\right\}, \tag{6}$$

the result of the time-domain integration of $g_{n>0}(t)\Gamma(t)$ will therefore correspond to all of the $n > 0$ terms in Eq. (1), nor is there any problem with the Fourier transformation to $g_{n>0}(t)$. Precisely this result is shown for the 1D parallel

plates in Fig. 1, and we see that it indeed matches the $n > 0$ terms from the analytical expression. To handle the $\omega = 0$ contribution, we begin with the real-ω $T = 0$ force expression, following our notation from the time-domain stress-tensor method [1, 2]:

$$F_i = \mathrm{Im}\,\frac{\hbar}{\pi}\int_0^\infty d\omega\; g_R(\omega)\Gamma_i(\omega), \tag{7}$$

where $g_R(\omega) = -i\omega$ is the weighting factor for the $\sigma = 0$ real ω contour and $\Gamma_i(\omega) = \Gamma_i^E(\omega) + \Gamma_i^H(\omega)$ is the surface-integrated stress tensor (electric- and magnetic-field contributions). From Eq. (1), the $\omega = 0$ contribution for $T > 0$ is then

$$\begin{aligned} F_{i,(n=0)} &= \lim_{\omega\to 0^+} \mathrm{Im}\left[\frac{\hbar}{\pi}\frac{1}{2}(-i\omega)\Gamma_i(\omega)\frac{2\pi k_\mathrm{B}T}{\hbar}\right] &(8)\\ &= \lim_{\omega\to 0^+} \mathrm{Re}\left[-\omega\Gamma_i(\omega)k_\mathrm{B}T\right]. &(9)\end{aligned}$$

(Notice that $\hbar$ cancels in the $\omega = 0$ contribution: this term dominates in the limit of large T where the fluctuations can be thought of as purely classical thermal fluctuations.) To relate Eq. (9) to what is actually computed in the FDTD method requires some care because of the way in which we transform to the $\omega(\xi)$ contour. The quantity $\Gamma_i^E(\omega)$ is proportional to an integral of $E_{ij}(\omega) = -i\omega G_{ij}(\omega)$, from Eq. (4). However, the $\omega(\xi)$ transformed system computes $\tilde\Gamma_i^E(\xi) \sim \tilde E_{ij}(\xi) = -i\xi\tilde G_{ij}(\xi)$, where $\tilde G(\xi)$ solves Eq. (3) with $\omega^2\varepsilon(\mathbf{r}) \to \xi^2(1 + \frac{i\sigma}{\xi})\varepsilon(\mathbf{r})$, but what we actually want is $-i\omega G_{ij}(\omega)|_{\omega=\omega(\xi)} = -i\omega(\xi)\tilde G_{ij}(\xi)$. Therefore, the correct $\omega = 0$ contribution is given by

$$\lim_{\omega\to 0^+}\Gamma_i^E(\omega) = \lim_{\xi\to 0^+}\frac{\omega(\xi)}{\xi}\tilde\Gamma_i^E(\xi) \tag{10}$$

Combined with $\omega(\xi)k_\mathrm{B}T$ factor from Eq. (9), this gives an $n = 0$ contribution of $\tilde\Gamma|_{\xi=0^+}$ multiplied by $-\omega(\xi)^2 k_\mathrm{B}T/\xi|_{\xi=0^+} = \sigma k_\mathrm{B}T$. This $\omega = 0$ term corresponds to a simple expression in the time domain, since $\tilde\Gamma|_{\xi=0^+}$ is simply the time integral of $\tilde\Gamma(t)$ and the coefficient $\sigma k_\mathrm{B}T$ is merely a constant. Therefore, while we originally integrated $g_{n>0}(t)\tilde\Gamma(t)$ to obtain the $n > 0$ contributions, the $n = 0$ contribution is included if we instead integrate:

$$[g_{n>0}(t) + \sigma k_\mathrm{B}T]\,\tilde\Gamma(t). \tag{11}$$

The term $[g_{n>0}(t) + \sigma k_\mathrm{B}T]$ generalizes the original $g(t)$ function from Ref. 1 to any $T \geq 0$.

We check Eq. (11) for the 1D parallel plate case in Fig. 1 against the analytical Lifshitz formula [25]. As noted above, the $g_{n>0}$ term (6) correctly gives the $n > 0$ terms, and we also see that the $\sigma k_\mathrm{B}T$ term gives the correct $n = 0$ contribution, and hence the total force is correct.

As another check, we consider a more complicated piston-like geometry Ref. 3, shown schematically in the inset of Fig. 2. Two square rods lie between two sidewalls, which we solve here for the 2D case of z-invariant fluctuations. At $T = 0$, such geometries exhibit an interesting non-monotonic variation of the force between the two blocks as a function of sidewall separation d [3, 21], which does not arise in the simple pairwise-interaction heuristic picture of the Casimir force. This can be seen in the solid lines of Fig. 2, where the non-monotonicity arises from a competition between forces from transverse-electric (TE, **E** in-plane) and transverse-magnetic (TM, **E** out-of-plane) polarizations [26], which can be explained by a method-of-images argument [21]. In Fig. 2, the solid lines are computed by a $T = 0$ frequency-domain boundary-element method (BEM) [7], whereas the circles are computed by the $T = 0$ FDTD method [1, 2], and both methods agree. We also compute the force at $T = 1 \times \pi c\hbar/k_\mathrm{B}a$ where the $\xi = 0^+$ term dominates. We see that the FDTD method with the $T > 0$ modification Eq. (11) (diamonds) agrees with the frequency-domain BEM results (dashed lines), where the latter simply use the Matsubara sum (1) to handle $T > 0$.

Interestingly, Fig. 2 shows that the non-monotonic effect disappears for $T = 1 \times \pi c\hbar/k_\mathrm{B}a$, despite the fact that the method-of-images argument of Ref. 21 ostensibly applies to the $\xi = 0^+$ quasi-static limit (which dominates at this large T) as well as to $\xi > 0$. The argument used the fact that TM fluctuations can be described by a scalar field with Dirichlet boundary conditions (vanishing at the metal), and in this case the sidewalls introduce opposite-sign mirror sources that reduce the interaction as d decreases; in contrast, TE corresponds to a Neumann scalar field (vanishing slope), which requires same-sign mirror sources that increase the interaction [21]. In Fig. 2, however, while the $T = 1 \times \pi c\hbar/k_\mathrm{B}a$ TM force still decreases as d decreases, the TE force no longer increases for decreasing d at $T = 1 \times \pi c\hbar/k_\mathrm{B}a$. The problem is that the image-source argument most directly applies to z-directed dipole sources in the scalar-field picture—electric J_z^E currents for TM and magnetic J_z^H currents for TE—while the situation for in-plane sources (corresponding to derivative of the scalar field from dipole-like sources) is more complicated [27]. For a sufficiently large T dominated by the $\xi = 0^+$ contribution (as here), we find numerically that the J_z^H sources

no longer contribute to the force as $\xi \to 0^+$. Intuitively, as $\xi \to 0^+$ a magnetic dipole produces nearly constant (wavelength $\to \infty$) field, which satisfies the Neumann conditions and hence is not affected by geometry. Instead, numerical calculations show that the TE $\xi = 0^+$ contribution is dominated by J_x^E sources and the corresponding electric stress-tensor terms, which turn out to slightly *decrease* in strength as d decreases. (A related effect is that, for small d, it can be observed in Fig. 2 that the $T = 1$ force is actually smaller than the $T = 0$ force, again due to the suppression of the TE contribution. Since the force diverges as $T \to \infty$, this means that the force changes non-monotonically with T at small d; a similar non-monotonic temperature dependence was previously observed for Dirichlet scalar-field fluctuations in a sphere-plate geometry [15].)

In contrast, if we consider the 3D constant cross-section problem with z-dependent fluctuations, corresponding to integrating $e^{ik_z z}$ fluctuations over k_z [20], then we find that the non-monotonic effect is preserved at all T. This is easily explained by the fact that, for perfect metals, $k_z \neq 0$ is mathematically equivalent to a problem at $k_z = 0$ and $\xi \to \sqrt{\xi^2 + k_z^2}$ [3, 28], and so the $n = 0$ Matsubara term still contains contributions equivalent to $\xi > 0$ in which the J_z^H mirror argument applies and the situation is similar to $T = 0$. In any case, this 2D disappearance of non-monotonicity seems unlikely to be experimentally relevant, because we find that it only occurs for $T \gtrsim 0.7 \times \pi c\hbar / k_{\mathrm{B}} a$, which for $a = 1\mu$m corresponds to $T \gtrsim 5000K$.

Thus, a simple (but not too simple) modification to our previous time-domain method allows off-the-shelf FDTD software to easily calculate Casimir forces at nonzero temperatures. Although the disappearance of non-monotonicity employed here as a test case appears unrealistic, recent predictions of other realistic geometry/material effects [12], combined with the fact that temperature effects in complex geometries are almost unexplored at present, lead us to hope that future work will reveal further surprising temperature effects that are observable in micromechanical systems. Although various authors have debated which model $\varepsilon(\omega)$ most accurately reflects experiments [10, 11, 17–19], computational methods such as the one here are independent of such debates, since any desired material can be inserted in the computation (using standard techniques to express material dispersion in FDTD [23]). For example, although the perfect metals used in our examples are obviously an artificial material, it has been argued that if the perfect metal is viewed as the limit of a Drude model then the $n = 0$ contribution should be omitted [10] for the TM mode (using our TE/TM convention)—in our computational method, this is accomplished simply by dropping the second term from Eq. (11) during the TM calculation (and it turns out that non-monotonicity still disappears in a similar manner).

This work was supported in part by the Singapore-MIT Alliance Computational Engineering Flagship program, by the Army Research Office through the ISN under Contract No. W911NF-07-D-0004, by US DOE Grant No. DE-FG02-97ER25308, and by the Defense Advanced Research Projects Agency (DARPA) under contract N66001-09-1-2070-DOD.

[1] A. W. Rodriguez, A. P. McCauley, J. D. Joannopoulos, and S. G. Johnson, Phys. Rev. A **80**, 012115 (2009).
[2] A. P. McCauley, A. W. Rodriguez, J. D. Joannopoulos, and S. G. Johnson, Phys. Rev. A **81**, 012119 (2010).
[3] A. Rodriguez, M. Ibanescu, D. Iannuzzi, J. D. Joannopoulos, and S. G. Johnson, Phys. Rev. A **76**, 032106 (2007).
[4] S. J. Rahi, T. Emig, N. Graham, R. L. Jaffe, and M. Kardar, Phys. Rev. D **80**, 085021 (2009).
[5] A. Lambrecht, P. A. Maia Neto, and S. Reynaud, New J. Phys. **8**, 243 (2006).
[6] S. Pasquali and A. C. Maggs, Phys. Rev. A. **79**, 020102(R) (2009).
[7] M. T. H. Reid, A. W. Rodriguez, J. White, and S. G. Johnson, Phys. Rev. Lett. **103**, 040401 (2009).
[8] S. G. Johnson (2010), preprint at http://arxiv.org/abs/1007.0966 (2010).
[9] M. Bostrom and B. E. Sernelius, Phys. Rev. Lett. **84**, 4757 (2000).
[10] K. A. Milton, J. Phys. A **37**, R209 (2004).
[11] J. S. Hoye, I. Brevik, J. B. Aarseth, and K. A. Milton, J. Phys. A: Math. Gen. **39**, 6031 (2006).
[12] A. W. Rodriguez, D. Woolf, A. P. McCauley, F. Capasso, J. D. Joannopoulos, and S. G. Johnson, Phys. Rev. Lett. **105**, 060401 (2010).
[13] C. Genet, A. Lambrecht, and S. Reynaud, International Journal of Modern Physics A **17**, 761 (2002).
[14] H. Haakh, F. Intravaia, and C. Henkel, Phys. Rev. A. **82**, 012507 (2010).
[15] A. Weber and H. Gies, Phys. Rev. Lett. **105**, 040403 (2010).
[16] M. Antezza, L. P. Pitaevskiĭ, S. Stringari, and V. B. Svetovoy, Phys. Rev. Lett. **97**, 223203 (2006).
[17] R. S. Decca, D. Lopez, E. Fischbach, G. L. Klimchitskaya, D. E. Krause, and V. M. Mostepanenko, Phys. Rev. D **75**, 077101 (2007).
[18] M. Masuda and M. Sasaki, Phys. Rev. Lett. **102**, 171101 (2009).
[19] A. O. Sushkov, W. J. Kim, D. A. R. Dalvit, and S. K. Lamoreaux, Nat. Phys. (2011), advanced online publication at http://dx.doi.org/10.1038/nphys1909 (2011).
[20] L. D. Landau, E. M. Lifshitz, and L. P. Pitaevskiĭ, *Statistical Physics Part 2*, vol. 9 (Pergamon, Oxford, 1980), 3rd ed.
[21] S. J. Rahi, A. W. Rodriguez, T. Emig, R. L. Jaffe, S. G. Johnson, and M. Kardar, Phys. Rev. A **77**, 030101(R) (2008).

[22] S. K. Lamoreaux, Rep. Prog. Phys. **68**, 201 (2005).
[23] A. Taflove and S. C. Hagness, *Computational Electrodynamics: The Finite-Difference Time-Domain Method* (Artech, Norwood, MA, 2005), 3rd ed.
[24] L. D. Landau and E. M. Lifshitz, *Statistical Physics: Part 1* (Butterworth-Heinemann, Oxford, 1980), 3rd ed.
[25] K. A. Milton, *The Casimir effect : physical manifestations of zero-point energy* (World Scientific, River Edge, NJ, 2001).
[26] A. Rodriguez, M. Ibanescu, D. Iannuzzi, F. Capasso, J. D. Joannopoulos, and S. G. Johnson, Phys. Rev. Lett. **99**, 080401 (2007).
[27] P. Rodriguez-Lopez, S. J. Rahi, and T. Emig, Phys. Rev. A **80**, 022519 (2009).
[28] T. Emig, R. L. Jaffe, M. Kardar, and A. Scardicchio, Phys. Rev. Lett. **96**, 080403 (2006).

Figures

FIG. 1: Comparison between FDTD (red circles) and the analytical Lifshitz formula [25] (blue line) for the Casimir force between perfect-metal plates in 1D with separation a. The $\omega = 0$ and $\omega \neq 0$ contributions to the Matsubara sum (1) are plotted separately, in addition to the total force. The straightforward method of including the $\coth(\hbar\omega/2kT)$ Boes-Einstein factor in the FDTD integration (green dashed line) gives an incorrect result because the $\omega = 0$ pole requires special handling.

FIG. 2: Comparison between FDTD (circles and diamonds) and BEM frequency domain (solid and dashed lines) calculation of the 2D Casimir force (z-invariant fluctuations) between two perfect-metal sidewalls (separation d), normalized by the proximity force approximation for the 2D parallel plates $F_{PFA} = \hbar c\zeta(3)/8\pi a^2$. At $T = 0$ (circles and solid lines) total force (black) varies non-monotonically with d, due to competition between TE (red) and TM (blue) polarizations [21]. At $T = 1 \times \pi c\hbar/k_{\mathrm{B}}a$ (dashed lines and diamonds) BEM and FDTD match, but the non-monotonicity disappears.

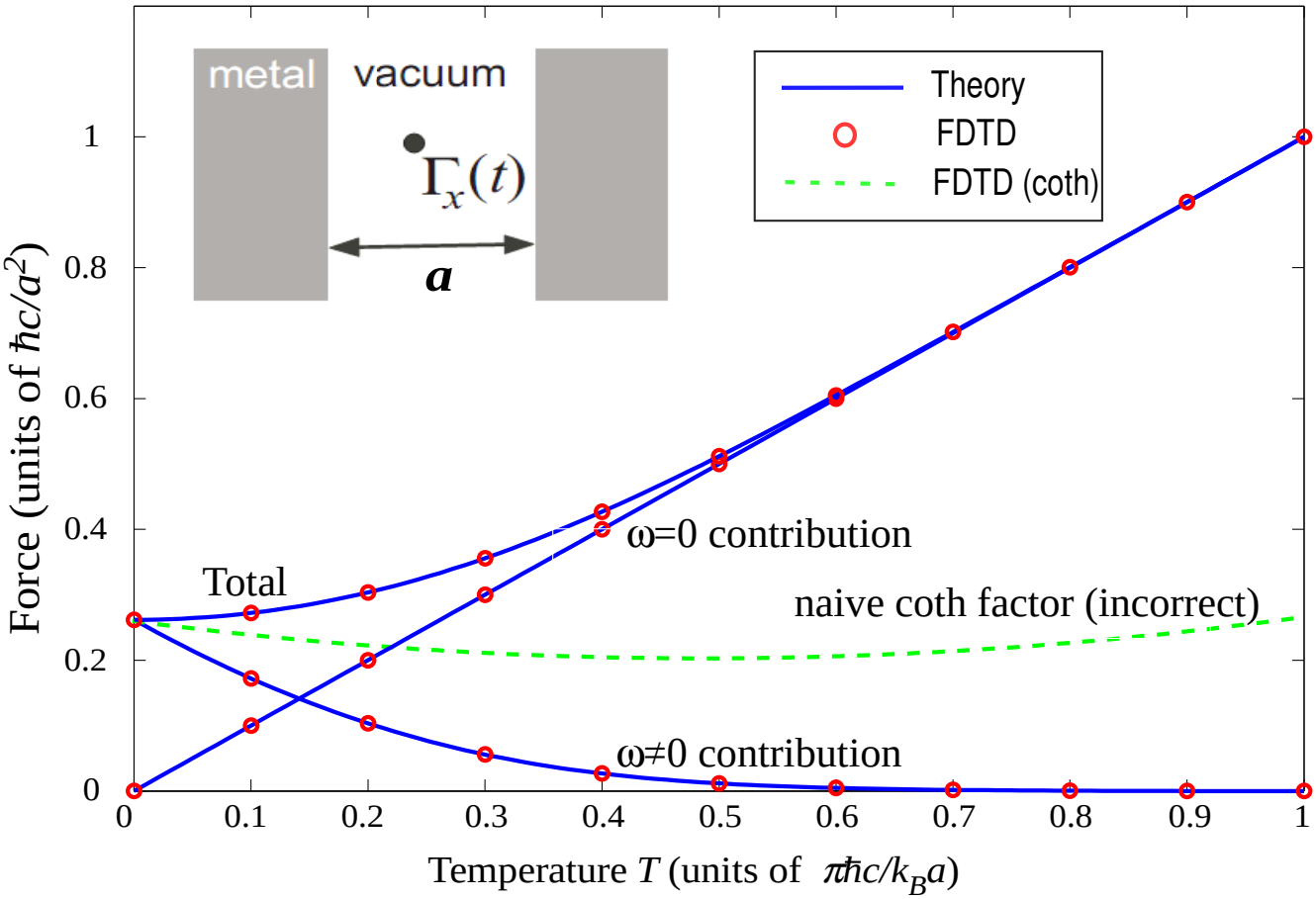

Figure 1 AYR1028 25Mar2011

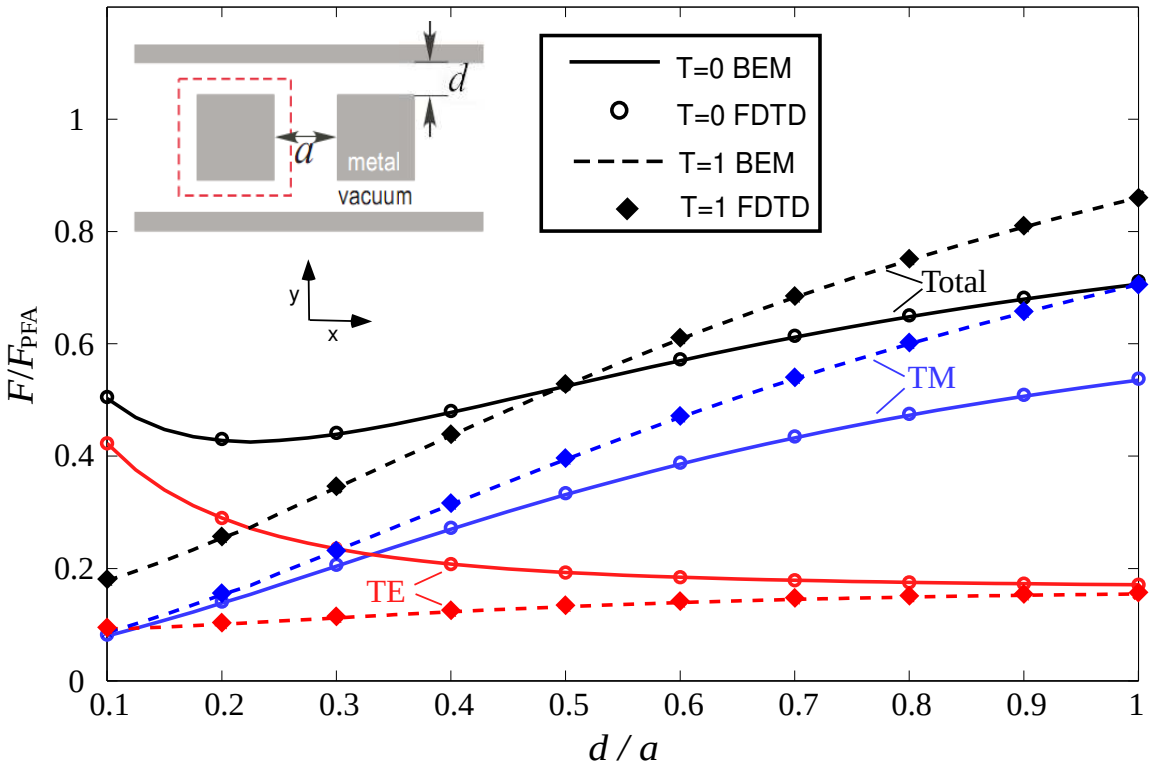

Figure 2 AYR1028 25Mar2011